The Company of Biologists

SHORT COMMUNICATION

Hydrodynamic properties of fin whale flippers predict maximum rolling performance

Paolo S. Segre[1,*], David E. Cade[1], Frank E. Fish[2], Jean Potvin[3], Ann N. Allen[4], John Calambokidis[4], Ari S. Friedlaender[5] and Jeremy A. Goldbogen[1]

ABSTRACT

Maneuverability is one of the most important and least understood aspects of animal locomotion. The hydrofoil-like flippers of cetaceans are thought to function as control surfaces that effect maneuvers, but quantitative tests of this hypothesis have been lacking. Here, we constructed a simple hydrodynamic model to predict the longitudinal-axis roll performance of fin whales, and we tested its predictions against kinematic data recorded by on-board movement sensors from 27 free-swimming fin whales. We found that for a given swimming speed and roll excursion, the roll velocity of fin whales calculated from our field data agrees well with that predicted by our hydrodynamic model. Although fluke and body torsion may further influence performance, our results indicate that lift generated by the flippers is sufficient to drive most of the longitudinal-axis rolls used by fin whales for feeding and maneuvering.

KEY WORDS: Fin whale, Roll, Swimming, Kinematics, Maneuvering

INTRODUCTION

Understanding the relationship between morphological design and locomotor performance remains a central challenge in the field of biomechanics (Webb, 1984). Simple physical models and engineering analogs have been used to approximate different aspects of terrestrial (Biewener, 2003), aerial (Ellington, 1984; Pennycuick, 1975) and aquatic locomotion (Alexander, 2005; Daniel, 1984), even though these models do not capture the full complexity of natural systems (Altshuler et al., 2005). Maneuvers, which by nature are rapid and transient, may also be amenable to simple modeling as a first approximation, and this approach could improve our understanding of the links between morphology and critical life functions such as defending territories, capturing prey or escaping predators.

Large aquatic animals provide a unique opportunity to study locomotor performance and maneuverability because they can be instrumented, allowing *in situ* body kinematics to be remotely measured (Goldbogen et al., 2013; Miller, 2004; Watanabe et al., 2015). The performance of this diverse assemblage of organisms is highly influenced by the anatomical geometry of the control

surfaces used to generate lift during swimming (Fish, 2002, 2004; Fish and Lauder, 2006). In whales and dolphins (Cetacea), these control surfaces include flukes and flippers with geometries and hydrodynamic properties similar to those of engineered wings (Fish, 2004; Weber et al., 2014). A central paradigm of cetacean locomotion is that posteriorly positioned flukes are oscillated to generate thrust (Fish et al., 2014), while the anteriorly located flippers create lift used for maneuvers, stability and the maintenance of body trim (Fish, 2002; Fish et al., 2003b; Weber et al., 2009). Given that their locomotion relies on separate propulsion and control surfaces (Fish, 2002), and the evidence that their vertebral design may limit flexibility (Long et al., 1997; Woodward et al., 2006), large cetaceans may behave more like rigid-hulled objects, and their maneuvering performance can be modeled as such.

A roll is a rotation about the longitudinal axis and is a common maneuver exhibited by many flying and swimming animals (Fish, 2002; Fish et al., 2003a, 2006, 2007; Norberg, 1990; Schilstra and Hateren, 1999). Rolls form the basis for more complex maneuvers, such as banked turns (Schilstra and Hateren, 1999), and are used as building blocks for intricate maneuvering trajectories. Rolling performance affects many functions including reorientation of the visual field (Goldbogen et al., 2013), prey capture and feeding (Fish, 2002; Fish et al., 2007), cleaning (Limbaugh, 1961), social interactions (McBride and Kritzler, 1951) and dislodging parasites (Fish et al., 2006; Weihs et al., 2007). Baleen whales in the family Balaenopteridae, or rorquals, frequently roll during feeding events (Goldbogen et al., 2006; Kot and Borda, 2014). Rorqual whales can perform 360 deg barrel rolls, but more often use 90 deg lateral rolls or 180 deg inverted rolls for feeding and maneuvering (Kot and Borda, 2014). It is unknown why rorquals roll during feeding, but given that these large whales depend on high prey density (Goldbogen et al., 2015), rolling is thought to increase the efficiency of foraging by facilitating prey capture (Goldbogen et al., 2013; Potvin et al., 2010).

It is hypothesized that rolling maneuvers are primarily controlled by the flippers, but few studies have examined this mechanism. We tested this hypothesis by developing a simple model that incorporates empirically measured hydrodynamic performance of fin whale (*Balaenoptera physalus*) flipper morphology (Weber et al., 2014) to predict rolling performance. The predictions made from the model were compared with kinematic data measured by multi-sensor tags attached to the body with suction-cups and equipped with inertial movement units.

MATERIALS AND METHODS
Hydrodynamic model

Using previously published morphological and hydrodynamic measurements of fin whales (Weber et al., 2014), we constructed a simple hydrodynamic model to predict longitudinal axis rotational

[1]Department of Biology, Hopkins Marine Station, Stanford University, Pacific Grove, CA 93950, USA. [2]Department of Biology, West Chester University, West Chester, PA 19383, USA. [3]Department of Physics, Saint Louis University, St Louis, MO 63103, USA. [4]Cascadia Research Collective, 218 ½ W. 4th Avenue, Olympia, WA 98501, USA. [5]Department of Fisheries and Wildlife, Marine Mammal Institute, Hatfield Marine Science Center, Oregon State University, Newport, OR 97365, USA.

*Author for correspondence (psegre@stanford.edu)

P.S.S., 0000-0002-2396-2670

acceleration (α; Fig. 1, Table 1):

$$\alpha = \frac{\tau}{I}, \tag{1}$$

where I is the moment of inertia and τ is the flipper-generated torque. Given the complex shape of a whale's body, we estimated the moment of inertia three ways: as a cylinder, as two half-ellipsoids joined at the base, and as two cones joined at the base (Fig. 1B), using the following equations:

$$I_{cylinder} = \frac{1}{2} m R_{body}^{2}, \tag{2}$$

$$I_{ellipsoid} = \frac{2}{5} m R_{body}^{2}, \tag{3}$$

$$I_{cones} = \frac{3}{10} m R_{body}^{2}, \tag{4}$$

where R_{body} is the radius of the body measured at the maximum width, and m is the mass estimated using the equation for northern hemisphere fin whales (Lockyer, 1976):

$$m = 0.0015 L_{body}^{3.46}. \tag{5}$$

The magnitude of the torque (τ) is calculated as:

$$\tau = R_{force} F_{total}, \tag{6}$$

where R_{force} is the radius at which the force is perpendicularly applied (Fig. 1A). Because the center of pressure along the surface of a balaenopterid flipper is not known, we approximated R_{force} as R_{body} plus half the length of the flipper ($L_{flipper}$). The total force applied (F_{total}) is the sum of the maximum upwards force (F_{up}) and the maximum downwards force (F_{down}) the flippers can produce on opposite sides of the body (see Fig. 1A, Table 1). These forces were calculated using the lift equation:

$$F = \frac{1}{2} \rho A C_{L} V^{2}, \tag{7}$$

where ρ is density, A is the planar area of the flipper, C_{L} is the coefficient of lift (measured empirically by Weber et al., 2014) and V is the velocity of the oncoming flow. The maximum torque is achieved when one flipper generates the maximum upwards force ($F_{max,up}$, $C_{L,max}$), and the other flipper generates the maximum downwards force ($F_{max,down}$, $C_{L,min}$; Fig. 1A). As the forces depend

on the velocity of the oncoming flow (V), we calculated the angular acceleration at swimming speeds of 1, 2, 3 and 4 m s^{-1}. This range of speeds is commonly used by foraging fin whales (Goldbogen et al., 2006), but remains well below the reported maximum for the species (10 m s^{-1}; Bose and Lien, 1989).

Each roll consists of an acceleration phase and deceleration phase. We estimated maximum angular velocity (ω) achieved during acceleration phases of 15, 45, 75, 105, 135 and 165 deg using the following equation:

$$\omega = \sqrt{2\alpha\theta + \omega_{i}^{2}}, \tag{8}$$

where α is assumed to be constant, θ is the angular deflection during the acceleration phase, and the initial angular velocity (ω_{i}) is zero (Halliday et al., 2014).

Because angular velocity is highly influenced by moment of inertia, at a given swimming speed the maximum angular velocity of the species is expected to be close to that of its smallest individuals (see Appendix for derivation). The inputs of the model, measured from a small adult fin whale, are reported in Table 1 and detailed predictions can be found in Table S1.

Roll velocity measurements

Between 2010 and 2015, we deployed digital acoustic recording tags (DTAGs; N=25, 124 h and 43 min; Johnson and Tyack, 2003) and Customized Animal Tracking Solutions (Queensland, Australia; Oberstdorf, Germany) tags (CATS; N=2, 24 min) on fin whales in both the Pacific Ocean (Southern California Bight) and the Atlantic Ocean (Stellwagen Bank). The whales were approached in a rigid-hulled inflatable boat and tagged using a 6 m carbon-fiber pole. The tags were affixed to the dorsal surface of the animal with suction-cups. The tags were equipped with accelerometers (DTAGs: 50, 200 or 500 Hz; CATS: 40 Hz), magnetometers (DTAGs: 50, 200 or 500 Hz; CATS: 40 Hz) and depth sensors (DTAGs 50, 200 or 500 Hz; CATS: 10 Hz). Additionally, the DTAGs included hydrophones (up to 64 kHz) while the CATS tags included onboard video cameras (720 pixels, 24 frames s^{-1}) and gyroscopes (40 Hz). After a period of time, the tags released from the whale and floated to the sea surface where they were retrieved.

This study was conducted in accordance with the US National Marine Fisheries Service Permitting Authority (permit no. 14534,
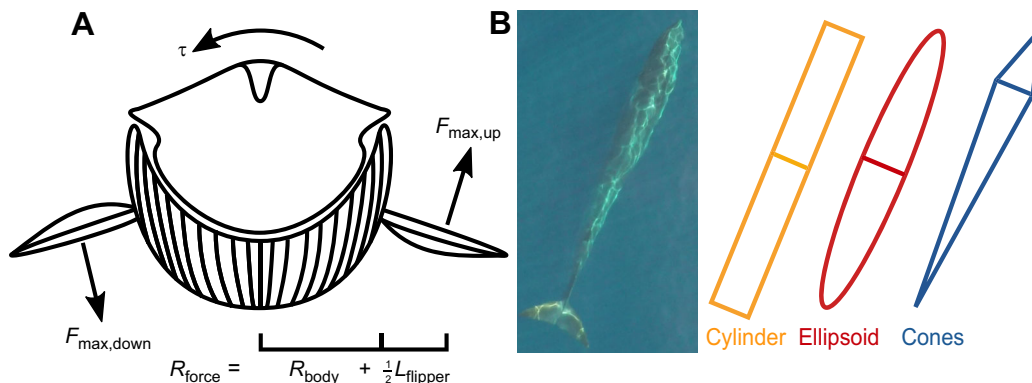
Fig. 1. A simple hydrodynamic model to predict roll performance in fin whales. (A) The whale was modeled as a rigid body and torque (τ) was calculated as the cross-product between the radius (R_{force}) and the total force produced. The radius was the sum of the radius of the body (R_{body}) and half the length of the flipper ($L_{flipper}$). The total force was the sum of the maximum upward force ($F_{max,up}$) produced by one flipper and the maximum downward force ($F_{max,down}$) produced by the other flipper. See Materials and methods. (B) An aerial view of a fin whale demonstrates the shape of the body. We used cylindrical, ellipsoid and conical models to estimate the moment of inertia about the longitudinal axis. The image was taken immediately before the whale performed a 90 deg roll while lunge feeding (Movie 1).

Table 1. Hydrodynamic model inputs

Parameter	Abbreviation	Value
Body length	L_{body}	14.4 m
Body diameter	D_{body}	2.63 m
Flipper area	A	0.1195 m^2
Flipper length	$L_{flipper}$	1.48 m
Maximum coefficient of lift	$C_{L,max}$	1.45
Minimum coefficient of lift	$C_{L,min}$	−1.04
Density	ρ	1024 kg m^{-3}

Data are from Weber et al. (2014).

issued to N. Cyr with B. Southall as chief scientist), the Channel Islands National Marine Sanctuary (permit no. 2010-004, issued to B. Southall), the Stellwaggen Bank National Marine Sanctuary (NMFS permit no. 775-185) and a consistency determination from the California Coastal Commission. All of the procedures were approved by the Institutional Animal Care and Use Committees at Stanford University and Oregon State University.

Roll angle about the longitudinal axis of the body was calculated from the accelerometers and smoothed using a low-pass Butterworth filter with a cutoff frequency of 0.15 Hz (0.5×0.3 Hz stroke frequency, from Goldbogen et al., 2006). Roll velocity was calculated by taking the derivative of a third-order interpolation spline fit to the roll angle. Pitch angles were calculated using the accelerometers and the swimming speed was estimated by calibrating measurements of the background noise recorded by the hydrophones or video camera microphones, against the orientation-corrected depth rate (for pitch angles >45 deg and depth >10 m; Goldbogen et al., 2006; Simon et al., 2012). A representative sequence of rolls is presented in Fig. 2. To account for differences in tag placement and hydrophone sensitivity, we used a separate calibration curve for each deployment. Six deployments were excluded from the analysis because there were few segments with steep pitch angles, or there was not a strong positive correlation between corrected depth rate and flow noise. The calibration curves for the remaining 21 deployments had an average correlation coefficient of 0.63±0.05 (mean±s.e.m.). Calculations were performed in MATLAB (MathWorks Inc., Natick, MA, USA) and Python (Python Software Foundation) programming languages.

We defined rolls as trajectories where the roll velocity starts and ends at zero, and the angle rolled was >45 deg. This stands in contrast with previous studies that identified rolls as rotational deviation from an upright, cruising posture and were intended to relate rolling behavior to feeding events (Goldbogen et al., 2006, 2013; Stimpert et al., 2007). To minimize the errors due to gimbal lock (Johnson and Tyack, 2003), we excluded rolls where the maximum pitch angle was >60 deg and <−60 deg. For each roll event, we measured the average swimming speed and the maximum instantaneous roll velocity. We compared the maximum angular velocity of rolls with acceleration phases of different durations (15, 45, 75, 105, 135 and 165±15 deg), with the predictions made with the hydrodynamic model.

RESULTS AND DISCUSSION

We identified 3199 rolls performed by 27 fin whales. Because our method of estimating swimming speed was only reliable at depths below 10 m, we discarded 1099 rolls. We discarded an additional 426 rolls where the estimate of swimming speed was not reliable. Of the remaining 1674 rolls performed by 21 whales, we identified 1567 rolls where the angular deflection (θ) was 90±45 deg, 86 rolls where the angular deflection was 180±45 deg, one roll where the
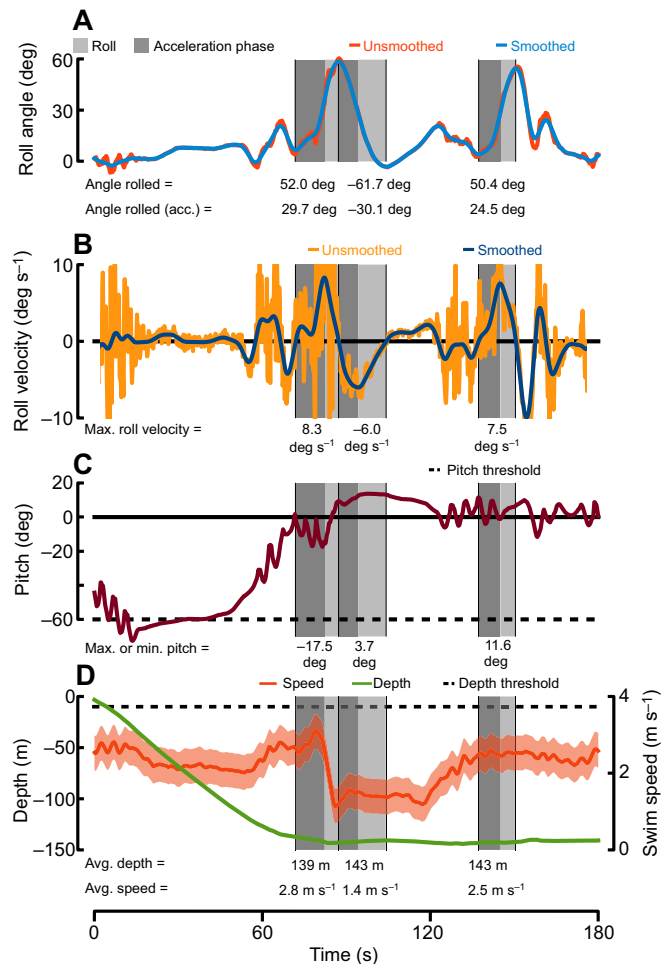
Fig. 2. An example of raw data collected from a free-swimming fin whale, demonstrating the search parameters used for identifying rolls. Three rolls of >45 deg were performed during a 180 s segment (gray bars; roll properties calculated from the graphs are listed underneath each bar). (A) Roll angle was calculated from the accelerometer data (red) and was smoothed with a low-pass Butterworth filter (blue; cutoff frequency 0.15 Hz). (B) Maximum roll velocity was calculated from the smoothed angular velocity (blue; unsmoothed velocity shown in orange). Smoothed roll velocity was used to determine the acceleration phases of each roll (dark gray bars). (C) Only rolls where the pitch was between 60 and −60 deg were included in the analysis. (D) Swimming speed (orange, with 95% confidence intervals shown) was estimated by measuring the level of the background noise recorded by the hydrophones or video camera microphones. This method of calculating swimming speed is only valid when the whale is at depths below 10 m (green).

angular deflection was 270±45 deg, and 16 rolls where the angular deflection was 360±45 deg. Additionally, we found four rolls where the angular deflection was >405 deg (Table S2).

The hydrodynamic model was not intended to predict exact roll velocity, and there are several mechanisms by which a whale could perform a slower-than-predicted roll. Whales have methods of modulating lift production by varying the angle of attack and sweep of the flippers (Cooper et al., 2008; Fish and Battle, 1995; Weber et al., 2014), and this introduces a behavioral component to the measured roll velocities. Additionally, rorqual whales change their shape during engulfment (Goldbogen et al., 2010), effectively increasing their diameter and mass and theoretically slowing their roll velocity (Goldbogen et al., 2013). To estimate the success of our model, we report the percentage of rolls that occur at or below the predicted maximum.

The majority of the measured rolls had angular velocities that were slower than the maximum predicted by the hydrodynamic model (Fig. 3). This suggests that the lift generated by the flippers is sufficient to drive the longitudinal-axis rolls used by fin whales for feeding and maneuvering. Of the 1661 rolls with acceleration phases ranging from 0 to 180 deg in duration, the conical model for moment of inertia predicted 92.8% of the measured roll velocities. This pattern held when the analysis was repeated using the more conservative estimates for moment of inertia (ellipsoid model: 85.4%; cylindrical model: 78.7%) and when using the 95% confidence intervals for swimming speed (conical model: 58.0% to 99.6%; ellipsoid model: 48.6% to 98.7%; cylindrical model: 41.8% to 96.8%). The true moment of inertia is probably best represented by the conical or ellipsoid model, or an intermediate version. The cylindrical model was the simplest model used, and likely resulted in overly conservative predictions of maximum roll velocity.

Despite its simplicity, our hydrodynamic model predicts the maximum angular velocity across a range of typical fin whale swimming speeds and roll durations. The range of recorded fin whale size and morphology is extensive (Goldbogen et al., 2010), with the largest individuals reaching lengths of up to 23 m and masses of up to 70,000 kg (Lockyer, 1976), and a substantial amount of temporal and geographic variation (Lockyer and Waters, 1986). The individual used for the hydrodynamic model calculations was smaller than average (14.4 m, estimated mass 15,300 kg; Weber et al., 2014). Because of the whale's smaller proportions and the inverse relationship of body size to maximum roll velocity, the calculations likely represent the upper boundary of adult fin whale rolling performance for a given swimming speed. One of the drawbacks to the tag data was that there was no information about tagged whale size or flipper morphology, and both are factors that would strongly influence the rolling performance calculated with the model. Body mass is directly related to the moment of inertia, whereas flipper area is related to the lift and thus the force necessary to effect the rotation. Although 133 of the 1661 rolls with acceleration phases lasting between 0 and 180 deg were faster than the maximum predicted by the conical hydrodynamic model, these rolls may have been performed either by smaller whales or by whales with relatively large flippers. We did find individual differences in roll performance among whales that could be a result of morphological variation. In spite of the high uncertainty, flow noise measurements remain a common and effective method for estimating swimming speed in whales (Laplanche et al., 2015; Simon et al., 2012). Although direct measurement of water flow is now possible through the use of paddle-wheels (Shepard et al., 2008; Watanabe et al., 2011), these have yet to be widely incorporated in suction-cup attached tags, where the placement of the tag on the animal is more variable. These uncertainties underscore the importance of developing new methods to measure the size, shape and swimming speed of tagged whales, if this type of hydrodynamic model is to be refined further.

Longitudinal-axis rolls are a well-documented and important component of rorqual whale locomotion (Goldbogen et al., 2006, 2013; Stimpert et al., 2007). Previous studies have suggested that fin whales mostly perform rolls of less than 90 deg (Goldbogen et al., 2006). Our data show that fin whales also perform inverted rolls (180 deg) and barrel rolls (360 deg). As would be expected by the size differences, fin whale rolls attain higher angular velocities (average across all swimming speeds: 39±3 deg s^{-1} for 16 rolls of 360±45 deg) than those previously measured in rolling blue whales
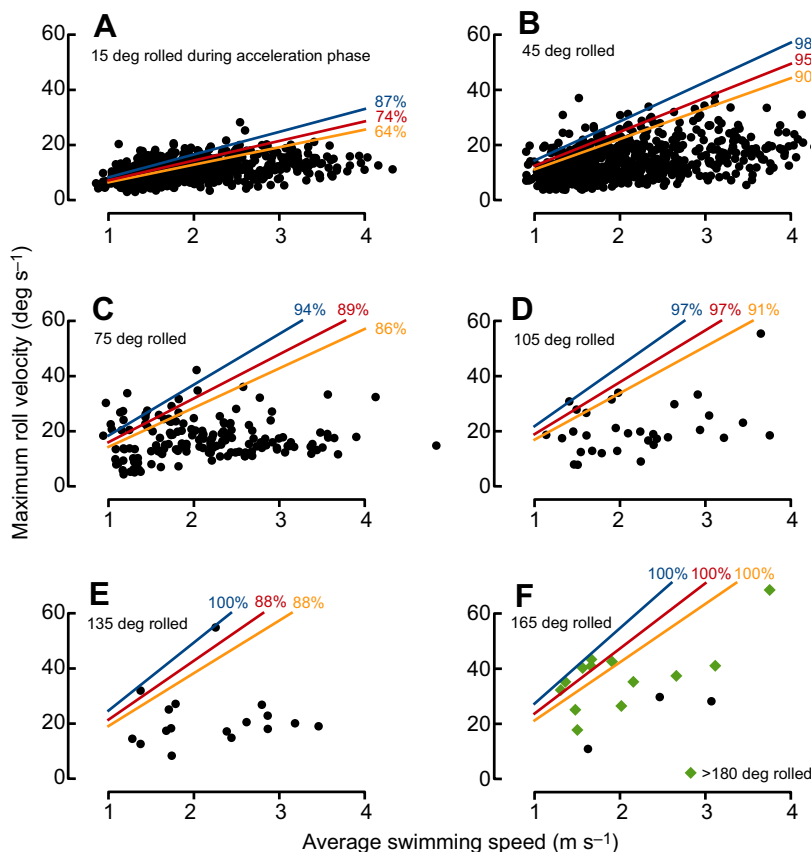
Fig. 3. The simple hydrodynamic model predicts maximum roll velocity of free-swimming fin whales. (A) Data for 706 rolls with an angular acceleration phase of 15±15 deg performed by 21 individual fin whales; 87.1% of the measured rolls had a maximum angular velocity that was below the maximum angular velocity predicted by the hydrodynamic model, using the conical approximation for moment of inertia (blue line). The predictions based on the ellipsoid (red line) and cylindrical (yellow line) models are also shown. Similar graphs are shown for: (B) 736 rolls with an angular acceleration phase of 45±15 deg performed by 21 fin whales; (C) 166 rolls with an angular acceleration phase of 75±15 deg performed by 20 fin whales; (D) 32 rolls with an angular acceleration phase of 105±15 deg performed by 10 fin whales; (E) 17 rolls with an angular acceleration phase of 135±15 deg performed by nine fin whales; and (F) four rolls with an angular acceleration phase of 165±15 deg performed by three fin whales. Additionally, 13 rolls with an acceleration phase >180 deg performed by eight whales are shown as green diamonds in F. Altogether, the conical model predicted 92.8% of the measured roll velocities with angular acceleration phases lasting between 0 and 180 deg.

(average: 33±8 deg s^{-1} for 33 rolls of 360 deg; from Goldbogen et al., 2013). As onboard tag databases expand to include more species and individuals, there will be an increased opportunity for rigorous comparisons of roll performance across body size and shape. Different rorqual species demonstrate a wide range of body sizes (minke whales to blue whales; Lockyer, 1976), body shapes (ellipsoid humpback whales versus conical fin whales; Goldbogen et al., 2010) and flipper morphology (humpback whale flippers versus other species; Fish and Battle, 1995; Miklosovic et al., 2004), which are all factors that impact maneuverability. A new development in tag design is the incorporation of multiple cameras that will allow for a detailed analysis of flipper and fluke kinematics during roll performance (Goldbogen et al., 2013). The use of cameras combined with the techniques of our current work will also help to elucidate the function of roll events during lunge feeding by providing simultaneous information regarding flipper orientation, visual cues, prey and gape (Goldbogen et al., 2016).

Cetacean flippers evolved from the tetrapod forelimb in whale ancestors as an adaptation for aquatic locomotion (Fish, 2002, 2004). Similar to engineered wings, flippers have a fusiform cross-section and a swept-back planform, and this morphological design enables enhanced lift generation relative to drag (Weber et al., 2009). The highly tapered, high aspect ratio flippers of fin whales yield greater lift-to-drag characteristics and a greater coefficient of lift compared with other large cetaceans that have more paddle-like flippers (Weber et al., 2014). The results from this study suggest that the flippers are capable of producing the long-axis torque used by fin whales to perform most rolls across a broad range of angular displacements. Although cetaceans may be able to generate additional torque to enhance roll performance through torsion of the flukes (Fish, 2002; Fish et al., 2006), this ability may be limited in larger cetacean species that have restricted spine and body flexibility (Long et al., 1997; Woodward, 2006). The extent to which the flippers and flukes work in concert to enhance maneuvering performance in large cetaceans requires further investigation; however, according to this model, the flippers can generate enough torque to effect the measured roll velocities.

Appendix
Scaling of maximum roll velocity versus body size
Inserting Eqns 5, 6, 7 and 8 into Eqn 1 yields:

$$I\alpha = I\frac{\omega^2}{2\theta} = R_{force}\frac{1}{2}\rho A C_L V^2, \qquad (A1)$$

or:

$$\omega = \sqrt{\frac{\theta R_{force}\rho A C_L}{I}} \cdot V, \qquad (A2)$$

resulting in the linear relationship between maximal roll rate (ω) and swimming speed (V) shown in Fig. 3. For a given swimming speed and roll angle (θ), assuming the seawater density (ρ) and maximum lift coefficient (C_L) are constant results in the relationship:

$$\omega \propto \sqrt{\frac{R_{force}A}{I}}. \qquad (A3)$$

Using Eqns 2–4 to substitute for I leads to:

$$\omega \propto \sqrt{\frac{R_{force}A}{mR_{body}^2}}. \qquad (A4)$$

If the morphological measurements R_{force}, R_{body}, A and m scale isometrically ($R_{force} \approx L_{body}$, $R_{body} \approx L_{body}$, $A \approx L_{body}^2$ and $m \approx L_{body}^3$), then maximum angular velocity would scale with the inverse of body length ($\omega \approx L_{body}^{-1}$). Alternatively, if R_{force}, R_{body} and A scale isometrically while mass scales allometrically ($m \approx L_{body}^{3.46}$; Eqn 5), then maximum angular velocity would scale with $L_{body}^{-1.23}$. If mass, body radius and flipper area scale allometrically ($m \approx L_{body}^{2.74}$, $R_{body} \approx R_{force} \approx W_{head} \approx L_{body}^{1.21}$: from Potvin et al., 2012; $A \approx P_{ant} \times P_{GW} \approx L_{body}^{2.07}$: from Goldbogen et al., 2010), then maximum angular velocity would scale with $L_{body}^{-0.94}$. Under a variety of scaling conditions the trends are the same: at a given swimming speed, fin whales with small body sizes have faster maximum rolling velocities. The individual used for the hydrodynamic model was smaller than average (14.4 m), and therefore the calculations presented likely represent the upper boundary of adult fin whale rolling performance.

References
Alexander, R. M. (2005). Models and the scaling of energy costs for locomotion. J. Exp. Biol. 208, 1645-1652.
Altshuler, D. L., Dickson, W. B., Vance, J. T., Roberts, S. P. and Dickinson, M. H. (2005). Short-amplitude high-frequency wing strokes determine the aerodynamics of honeybee flight. Proc. Natl. Acad. Sci. USA 102, 18213-18218.
Biewener, A. A. (2003). Animal Locomotion. Oxford: Oxford University Press.
Bose, N. and Lien, J. (1989). Propulsion of a fin whale (Balaenoptera physalus): why the fin whale is a fast swimmer. Proc. R. Soc. B Biol. Sci. 237, 175-200.
Cooper, L. N., Sedano, N., Johansson, S., May, B., Brown, J. D., Holliday, C. M., Kot, B. W. and Fish, F. E. (2008). Hydrodynamic performance of the minke whale (Balaenoptera acutorostrata) flipper. J. Exp. Biol. 211, 1859-1867.
Daniel, T. L. (1984). Unsteady aspects of aquatic locomotion. Integr. Comp. Biol. 24, 121-134.
Ellington, C. P. (1984). The aerodynamics of hovering insect flight. I. the quasi-steady analysis. Philos. Trans. R. Soc. B Biol. Sci. 305, 1-15.
Fish, F. E. (2002). Balancing requirements for stability and maneuverability in cetaceans. Integr. Comp. Biol. 42, 85-93.
Fish, F. E. (2004). Structure and mechanics of nonpiscine control surfaces. J. Ocean. Eng. 29, 605-621.

Fish, F. E. and Battle, J. M. (1995). Hydrodynamic design of the humpback whale flipper. *J. Morphol.* **225**, 51-60.

Fish, F. E. and Lauder, G. V. (2006). Passive and active flow control by swimming fishes and mammals. *Annu. Rev. Fluid Mech.* **38**, 193-224.

Fish, F. E., Hurley, J. and Costa, D. P. (2003a). Maneuverability by the sea lion *Zalophus californianus*: turning performance of an unstable body design. *J. Exp. Biol.* **206**, 667-674.

Fish, F. E., Peacock, J. E. and Rohr, J. J. (2003b). Stabilization mechanism in swimming odontocete cetaceans by phased movements. *Mar. Mamm. Sci.* **19**, 515-528.

Fish, F. E., Nicastro, A. J. and Weihs, D. (2006). Dynamics of the aerial maneuvers of spinner dolphins. *J. Exp. Biol.* **209**, 590-598.

Fish, F. E., Bostic, S. A., Nicastro, A. J. and Beneski, J. T. (2007). Death roll of the alligator: mechanics of twist feeding in water. *J. Exp. Biol.* **210**, 2811-2818.

Fish, F. E., Legac, P., Williams, T. M. and Wei, T. (2014). Measurement of hydrodynamic force generation by swimming dolphins using bubble DPIV. *J. Exp. Biol.* **217**, 252-260.

Goldbogen, J. A., Calambokidis, J., Shadwick, R. E., Oleson, E. M., McDonald, M. A. and Hildebrand, J. A. (2006). Kinematics of foraging dives and lunge-feeding in fin whales. *J. Exp. Biol.* **209**, 1231-1244.

Goldbogen, J. A., Potvin, J. and Shadwick, R. E. (2010). Skull and buccal cavity allometry increase mass-specific engulfment capacity in fin whales. *Proc. R. Soc. B Biol. Sci.* **277**, 861-868.

Goldbogen, J. A., Calambokidis, J., Friedlaender, A. S., Francis, J., DeRuiter, S. L., Stimpert, A. K., Falcone, E. and Southall, B. L. (2013). Underwater acrobatics by the world's largest predator: 360° rolling manoeuvres by lunge-feeding blue whales. *Biol. Lett.* **9**, 20120986.

Goldbogen, J. A., Hazen, E. L., Friedlaender, A. S., Calambokidis, J., DeRuiter, S. L., Stimpert, A. K. and Southall, B. L. (2015). Prey density and distribution drive the three-dimensional foraging strategies of the largest filter feeder. *Funct. Ecol.* **29**, 951-961.

Goldbogen, J., Cade, D., Calambokidis, J., Stimpert, A. and Friedlaender, A. (2016). Insights into the underwater behavior, species interactions, and biomechanics of baleen whales using suction-cup attached video and inertial sensors. *FASEB J.* **30**, 90-93.

Halliday, D., Resnick, R. and Walker, J. (2014). *Fundamentals of Physics*, 10th edn. New York, NY: John Wiley and Sons, Inc.

Johnson, M. P. and Tyack, P. L. (2003). A digital acoustic recording tag for measuring the response of wild marine mammals to sound. *IEEE J. Ocean. Eng.* **28**, 3-12.

Kot, B. W., Sears, R., Zbinden, D. and Borda, E. (2014). Rorqual whale (Balaenopteridae) surface lunge-feeding behaviors: Standardized classification, repertoire diversity, and evolutionary analyses. *Mar. Mamm. Sci.* **30**, 1335-1357.

Laplanche, C., Marques, T. A. and Thomas, L. (2015). Tracking marine mammals in 3D using electronic tag data. *Methods Ecol. Evol.* **6**, 987-996.

Limbaugh, C. (1961). Observations on the California sea otter. *J. Mamm.* **42**, 271-273.

Lockyer, C. (1976). Body weights of some species of large whales. *ICES J. Mar. Sci.* **36**, 259-273.

Lockyer, C. and Waters, T. (1986). Weights and anatomical measurements of northeastern Atlantic fin (*Balaenoptera physalus*, Linnaeus) and Sei (*B . borealis*, Lesson) whales. *Mar. Ecol. Prog. Ser.* **2**, 169-185.

Long, J. H., Pabst, D. A., Shepherd, W. R. and McLellan, W. A. (1997). Locomotor design of dolphin vertebral columns: bending mechanics and morphology of *Delphinus delphis*. *J. Exp. Biol.* **200**, 65-81.

McBride, A. F. and Kritzler, H. (1951). Observations on pregnancy, parturition, and postnatal behavior in the bottlenose dolphin. *J. Mammal.* **32**, 251-266.

Miklosovic, D. S., Murray, M. M., Howle, L. E. and Fish, F. E. (2004). Leading-edge tubercles delay stall on humpback whale (*Megaptera novaeangliae*) flippers. *Phys. Fluids* **16**, L39.

Miller, P. J. O. (2004). Swimming gaits, passive drag and buoyancy of diving sperm whales *Physeter macrocephalus*. *J. Exp. Biol.* **207**, 1953-1967.

Norberg, U. M. (1990). *Vertebrate Flight: Mechanics, Physiology, Morphology, Ecology and Evolution*. Berlin: Springer-Verlag.

Pennycuick, C. J. (1975). Mechanics of flight. In *Avian Biology* (ed. D. S. Farner, J. R. King and K. C. Parkes), pp. 1-75. London: Academic Press.

Potvin, J., Goldbogen, J. A. and Shadwick, R. E. (2010). Scaling of lunge feeding in rorqual whales: An integrated model of engulfment duration. *J. Theor. Biol.* **267**, 437-453.

Schilstra, C. and Hateren, J. H. (1999). Blowfly flight and optic flow. I. Thorax kinematics and flight dynamics. *J. Exp. Biol.* **202**, 1481-1490.

Shepard, E. L. C., Wilson, R. P., Liebsch, N., Quintana, F., Gómez Laich, A. and Lucke, K. (2008). Flexible paddle sheds new light on speed: a novel method for the remote measurement of swim speed in aquatic animals. *Endanger. Species Res.* **4**, 157-164.

Simon, M., Johnson, M. and Madsen, P. T. (2012). Keeping momentum with a mouthful of water: behavior and kinematics of humpback whale lunge feeding. *J. Exp. Biol.* **215**, 3786-3798.

Stimpert, A. K., Wiley, D. N., Au, W. W. L., Johnson, M. P. and Arsenault, R. (2007). "Megapclicks": acoustic click trains and buzzes produced during night-time foraging of humpback whales (*Megaptera novaeangliae*). *Biol. Lett.* **3**, 467-470.

Watanabe, Y. Y., Sato, K., Watanuki, Y., Takahashi, A., Mitani, Y., Amano, M., Aoki, K., Narazaki, T., Iwata, T., Minamikawa, S. et al. (2011). Scaling of swim speed in breath-hold divers. *J. Anim. Ecol.* **80**, 57-68.

Watanabe, Y. Y., Goldman, K. J., Caselle, J. E., Chapman, D. D. and Papastamatiou, Y. P. (2015). Comparative analyses of animal-tracking data reveal ecological significance of endothermy in fishes. *Proc. Natl. Acad. Sci. USA* **112**, 6104-6109.

Webb, P. W. (1984). Body form, locomotion and foraging in aquatic vertebrates. *Am. Nat.* **24**, 107-120.

Weber, P. W., Howle, L. E., Murray, M. M. and Fish, F. E. (2009). Lift and drag performance of odontocete cetacean flippers. *J. Exp. Biol.* **212**, 2149-2158.

Weber, P. W., Howle, L. E., Murray, M. M., Reidenberg, J. S. and Fish, F. E. (2014). Hydrodynamic performance of the flippers of large-bodied cetaceans in relation to locomotor ecology. *Mar. Mamm. Sci.* **30**, 413-432.

Weihs, D., Fish, F. E. and Nicastro, A. J. (2007). Mechanics of remora removal by dolphin spinning. *Mar. Mamm. Sci.* **23**, 707-714.

Woodward, B. L. (2006). Locomotory strategies, dive dynamics, and functional morphology of the mysticetes: Using morphometric, osteology, and DTAG data to compare swim performance in four species. PhD Dissertation, University of Maine, Orono, ME, USA.

Woodward, B. L., Winn, J. P. and Fish, F. E. (2006). Morphological specializations of baleen whales associated with hydrodynamic performance and ecological niche. *J. Morphol.* **267**, 1284-1294.